Available online at www.sciencedirect.com
SCIENCE DIRECT
Thermochimica Acta 442 (2006) 67–73
thermochimica acta
www.elsevier.com/locate/tca

Thermo-physical properties of epoxy nanocomposites reinforced by carbon nanotubes and vapor grown carbon fibers

Hiroaki Miyagawa *, Michael J. Rich, Lawrence T. Drzal

Composite Materials and Structures Center, Department of Chemical Engineering and Materials Science, College of Engineering, Michigan State University, East Lansing, MI 48824-1226, USA

Available online 21 February 2006

Abstract

In this study, the thermo-physical properties of epoxy nanocomposites reinforced by fluorinated single wall carbon nanotubes (FSWCNT) and vapor grown carbon fibers (VGCF) were investigated. A sonication technique using a suspension of FSWCNT and VGCF in acetone was utilized to process nanocomposites in anhydride-cured epoxy. The viscoelastic properties of the nanocomposites were measured with dynamic mechanical analysis. The glass transition temperature decreased approximately 30 °C with an addition of 0.14 vol.% (0.2 wt.%) FSWCNT. The depression in T_g is attributed to non-stoichiometric balance of the epoxy matrix caused by the fluorine on single wall carbon nanotubes. The correct amount of the anhydride curing agent needed to achieve stoichiometry was experimentally determined by DMA measurements. After adjusting the amount of the anhydride curing agent for stoichiometry, the storage modulus of the epoxy at room temperature increased 0.63 GPa with the addition of only 0.21 vol.% (0.30 wt.%) of FSWCNT, a 20% improvement compared with the anhydride-cured neat epoxy. For VGCF, the storage modulus at room temperature increased 0.48 GPa with the addition of only 0.94 vol.% (1.5 wt.%) and then reached a plateau for larger amounts of VGCF. To understand the influence of VGCF on thermo-physical properties, the microstructure of the nanocomposites was interrogated using transmission electron microscopy (TEM). This study discusses the chemical effects of fluorine on matrix properties and the effect of stoichiometric balance on the thermo-physical properties of nanocomposites.

Keywords: Dynamic mechanical analysis; Epoxy nanocomposites; Single wall carbon nanotubes; Sonication; Vapor grown carbon fibers

1. Introduction

Owing to their splendid elastic modulus and strength, the utility of using carbon nanotubes (CNT) as reinforcements in organic polymers began when CNT were discovered by Iijima in 1991 [1–7]. One major concern affecting the usage of CNT for engineering applications is its high cost compared to other nano-reinforcements, such as clay nanoplatelets. Alternately, vapor grown carbon fibers (VGCF) are also attracting increasing attention as nano-reinforcements due to much lower cost, although some mechanical properties of VGCF may be inferior to those of CNT. In some cases the reinforcing effects of the CNT and VGCF have not been maximized due to the inhomogeneous dispersion of these materials in the polymer matrix.

In this study, epoxy matrix nanocomposites reinforced by fluorinated single wall carbon nanotubes (FSWCNT) and VGCF were prepared. The morphologies of FSWCNT and VGCF in the as-received condition and after incorporation in an anhydride-cured epoxy matrix were observed by transmission electron microscopy. The effect of FSWCNT and VGCF loading on the viscoelastic properties of the nanocomposites was determined by dynamic mechanical analysis (DMA).

2. Experimental

2.1. Materials

2.1.1. Fluorinated single wall carbon nanotubes

Fluorinated single wall carbon nanotubes (Carbon Nanotechnologies Inc., Houston TX) were blended in the epoxy using a

Abbreviations: CNT, carbon nanotubes; CVD, chemical vapor deposition; DGEBF, diglycidyl ether of bisphenol F; DMA, dynamic mechanical analysis; FSWCNT, fluorinated single wall carbon nanotubes; HOPG, highly ordered pyrolytic graphite; HR-TEM, high resolution TEM; MTHPA, methyltetrahydrophthalic-anhydride; MWCNT, multi wall carbon nanotubes; SWCNT, single wall carbon nanotubes; phr, parts per hundred resin; TEM, transmission electron microscopy; T_g, glass transition temperature; VGCF, vapor grown carbon fibers; XPS, X-ray photoelectron spectroscopy

* Corresponding author. Present address: School of Packaging, Michigan State University, East Lansing, MI 48824-1223, USA. Tel.: +1 517 432 4384; fax: +1 517 353 8999.
E-mail address: miyagaw2@egr.msu.edu (H. Miyagawa).

0040-6031/$ – see front matter © 2006 Elsevier B.V. All rights reserved.
doi:10.1016/j.tca.2006.01.016

sonication technique [8]. The vendor reports a fluorination yield of at least 10 wt.% of fluorine, which equals a fluorine/carbon ratio of 0.08 [9]. FSWCNT retain much of their thermal conductivity and mechanical properties, since no carbon atoms are displaced during the fluorination, and consequently their structure is still defect-free. Kudin et al. [10] have concluded from the computed elastic constants that the stiffness of CNT is not affected by addition of large amounts of fluorine. Generally, untreated single wall carbon nanotubes (SWCNT) agglomerate via van der Waals forces to form a bundle that is extremely difficult to separate into individual SWCNT during the processing of SWCNT-reinforced nanocomposites. The supplier reports that SWCNT are typically about 100–1000 nm in length, whereas bundles are far longer than any individual SWCNT [11]. Mechanical characteristics of epoxy nanocomposites reinforced by untreated SWCNT report more than 1.0 wt.% SWCNT were used to improve the elastic modulus [12,13]. However, when the aspect ratio of SWCNT in these studies is considered, the theoretical reinforcing effect predicted by Tandon and Weng [14], Halpin and Tsai [15], and Hui and Shia [16] has not been achieved, which can be attributed to aggregation of the nanotubes. Fluorination disrupts the van der Waals forces between the nanotubes and increases the solubility of SWCNT in solvents such as alcohols and ketones, which leads to a greater degree of dispersion in these solutions. It is expected that the fluorine treatment will lead to greater bundle separation and dispersion of CNT in the polymer matrix and produce greater increases in the elastic modulus of the nanocomposites made with these materials.

2.1.2. Vapor grown carbon fibers

A commercially available VGCF [17], obtained from Applied Sciences Inc. (Cedarville OH), were evaluated in this study. PR-19-PS is pyrolytically stripped VGCF, in which polyaromatic hydrocarbons have been removed from the surface. PR-19-PS has a CVD carbon layer on the surface having a surface area of 20–30 m^2/g as measured by nitrogen adsorption. The outside diameter and the length of PR-19-PS are 100–200 nm and 30–100 μm, respectively. The density of VGCF was approximately 1.95 g/cm^3. The supplier reports that the elastic modulus is approximately 500 GPa.

2.1.3. Anhydride-cured epoxy

The epoxy resin was diglycidyl ether of bisphenol F (DGEBF), Epon 862 (Resolution Performance Products, Houston TX, epoxide equivalent weight = 172) processed with the anhydride curing agent methyltetrahydrophthalic-anhydride (MTHPA), Aradur^{TM} HY 917 (Huntsman Advanced Materials Americas Inc., Brewster, NY, equivalent weight = 159) and the accelerator 1-methylimidazole (DY 070, Huntsman Advanced Materials Americas Inc.). The mixing ratio for the neat epoxy was 100 parts by weight DGEBF to 92.7 parts MTHPA to 1.0 part imidazole. To fabricate the anhydride-cured FSWCNT/epoxy nanocomposites, up to 0.36 vol.% (0.5 wt.%) FSWCNT were sonicated in acetone for 5 h using a solution concentration of more than 1 L of acetone to 1 g of FSWCNT. Similarly for epoxy/VGCF nanocomposites, up to 2.5 vol.% (4.0 wt.%) VGCF were sonicated in acetone for 2 h using a solution concentration of more than 100 L of acetone to 10 g of VGCF. DGEBF was then added to the solution and mixed with a magnetic stirrer for an additional hour. The acetone was removed from the mixture by vacuum extraction at 100 °C for 24 h, after which time MTHPA and imidazole were blended in the solution with a magnetic stirrer. Previous work on clay/epoxy nanocomposites demonstrated that the acetone is fully removed and has no chemical effect on the system [8]. The specimens were cured at 80 °C for 4 h followed by 160 °C for 2 h.

2.2. Transmission electron microscopy

As-received FSWCNT were sonicated in acetone for 5 h, and then deposited onto a lacey carbon film substrate grid for evaluation by TEM. The nanocomposite samples were sectioned at room temperature using an ultramicrotome fitted with a diamond knife having an included angle of 4°. Thin sections of approximately 100 nm thick were obtained for TEM observations. A JEOL 2200FS TEM with a field emission filament operated at 200 kV accelerating voltage or a JEOL 100CX TEM with LaB_6 filament at 120 kV accelerating voltage was used to collect bright-field TEM images of the epoxy nanocomposites.

2.3. Dynamic mechanical analysis

Dynamic mechanical properties were measured with a TA Instruments DMA 2980 operating in the three-point bending mode at a frequency of 1.0 Hz. The amplitude and the static force were 75 μm and 1.0 N, respectively. Data were collected from room temperature of 27 °C to 170 °C at a scanning rate of 2 °C/min. DMA specimens were cut by a wet diamond saw in the form of rectangular bars of nominal dimensions: 2.2 (±2.0) mm × 12 (±1.5) mm × 50 mm. A minimum of 3 specimens of each composition were tested.

2.4. X-ray photoelectron spectroscopy

The surface chemistry of the VGCF was determined by X-ray photoelectron spectroscopy (XPS) using a PHI 5400 ESCA spectrometer (Physical Electronics, Eden Prairie MN). All measurements took place at operating pressures of less than 5×10^{-8} Torr. The samples were irradiated with a non-monochromatic Mg X-ray source (1253.6 eV) operating at 300 W with a take off angle of 45°. A pass energy of 187.85 eV was used for survey scans (0–1100 eV) and elemental regional scans were acquired with a pass energy of 29.35 eV. The O1s spectral envelope was deconvoluted with a non-linear least squares curve-fitting program (Multipak, Physical Electronics, Eden Prairie MN) using a Gaussian–Lorentzian peak shape. Peaks were assigned based on the assumption of a 1.5 eV chemical shift per bond to oxygen. The main oxygen peak was fixed to a binding energy of 533.6 eV.

3. Results and discussion

3.1. Transmission electron microscopy

Fig. 1 shows the bright field image of FSWCNT recorded by TEM. The diameter of the FSWCNT were recorded as 1.1 nm. In this TEM micrograph, the bundles of the Fluorinated-SWCNT were recorded to be typically smaller than the untreated SWCNT. The density of the FSWCNT was calculated using known values for highly ordered pyrolytic graphite (HOPG). Based on the density at 2.1 g/cm^3 with a d-spacing of HOPG at approximately 0.34 nm, and an assumed nanotube thickness of 0.3 nm, the density of FSWCNT was calculated to be approximately 1.7 g/cm^3. In the nanocomposites, the FSWCNT could not be recorded by TEM which indicates that the nanotubes were well separated and dispersed.

Fig. 2 shows a low magnification TEM micrograph revealing the dispersion of 2.5 vol.% (4.0 wt.%) PR-19-PS VGCF in the anhydride-cured epoxy matrix. The VGCF were randomly-oriented in the nanocomposites, showing both the transverse cross section of the VGCF as well as several axial sections as indicated by black arrows. For all weight fraction nanocomposites processed in this study the VGCF did not form aggregated bundles and were recorded to be homogeneously dispersed in the anhydride-cured epoxy matrix. The level of adhesion between untreated PR-19-PS VGCF and the epoxy matrix was weak as indicated by bright areas (white arrows in Fig. 2) where debonding is evident.

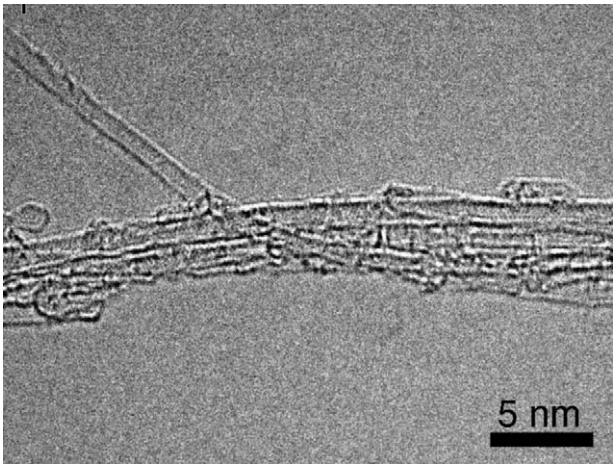

Fig. 1. High magnification TEM micrograph depicting sonicated FSWCNT before mixing with DGEBF.

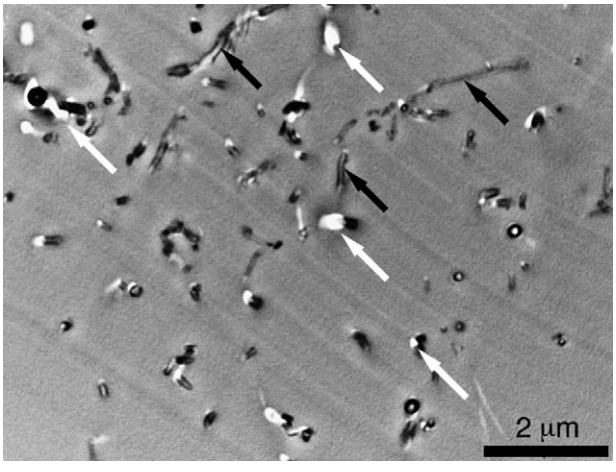

Fig. 2. Low magnification TEM micrograph of anhydride-cured epoxy nanocomposites reinforced by 2.5 vol.% (4.0 wt.%) PR-19-PS VGCF.

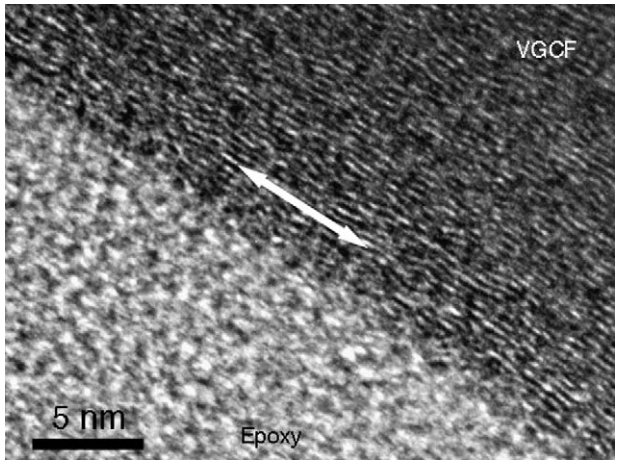

Fig. 3. HR-TEM micrograph depicting graphene layers of PR-19-PS VGCF. Arrow indicates fiber axial orientation.

Fig. 3 shows a high resolution HR-TEM micrograph revealing the graphene layers of VGCF dispersed in the epoxy matrix. The fiber direction is indicated by the white arrow showing that the graphene layers are oriented along the fiber longitudinal axis. It is known that graphene sheets have an elastic modulus in the a-b plane that is approximately 1 TPa, and the transverse elastic modulus perpendicular to the a-b plane is much lower than 1 TPa [18]. The graphene layers are oriented to the longitudinal fiber axis in VGCF as seen in Fig. 3. It can be expected that the elastic modulus of nanocomposites will be greatly increased with the addition of the high modulus VGCF. The d-spacing of the graphene layers of VGCF was measured as 0.34 nm, which is almost the same as those of graphite platelets and multi-wall carbon nanotubes (MWCNT).

3.2. DMA evaluations

Fig. 4 presents the graphical results of the DMA evaluation of the anhydride-cured FSWCNT/epoxy nanocomposites. The MTHPA was employed stoichiometrically with the neat DGEBF epoxy at 92.7 parts per hundred resin (phr). The same mixing ratio of epoxy was used to process FSWCNT nanocomposites in this figure. The storage modulus at 30 °C increased with up to 0.21 vol.% (0.3 wt.%) FSWCNT as shown, in Fig. 4(a). The symmetric peak of the loss factor, tan δ, in Fig. 4(b) indicates complete cure of the anhydride-cured epoxy matrix. The glass transition temperature was assigned as the temperature at peak maximum of tan δ as shown in Fig. 4(b). It can also be observed that the glass transition temperature decreased with increasing content of FSWCNT in the nanocomposite. The 0.21 vol.%

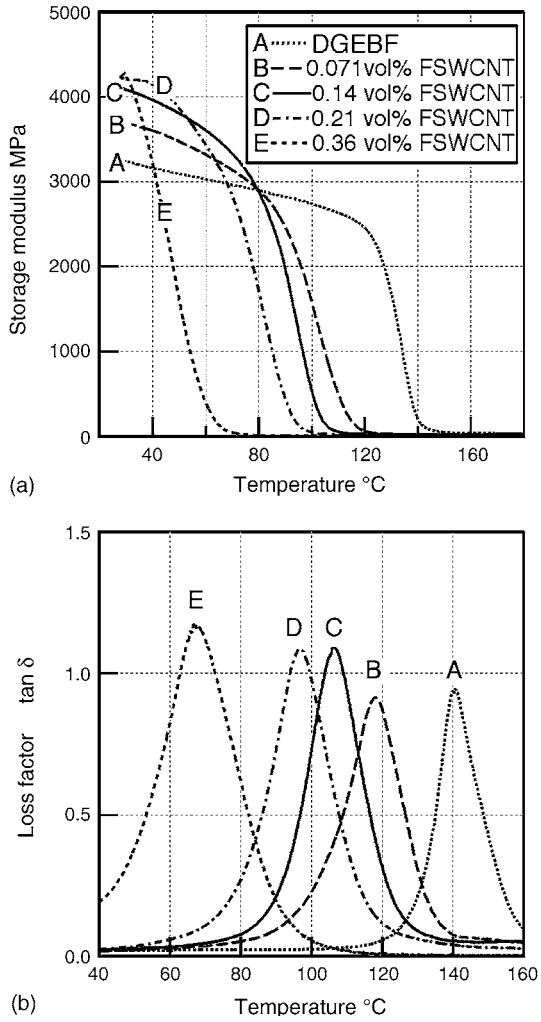

Fig. 4. DMA measurements for anhydride-cured FSWCNT/epoxy nanocomposites. (a) Storage modulus. (b) Loss factor.

FSWCNT nanocomposite exhibited a glass transition temperature near room temperature, which is a large variance from the neat, unfilled epoxy T_g of ~140 °C.

Unfilled symbols in Fig. 5 present the storage modulus of FSWCNT/epoxy nanocomposites, where the same mixing ratio of epoxy was used to process FSWCNT nanocomposites, as a function of volume percent FSWCNT measured at 30 °C by DMA. The storage modulus of FSWCNT/epoxy nanocomposites exhibited an almost linear increase with increasing FSWCNT content up to 0.21 vol.%. For the 0.36 vol.% (0.5 wt.%) nanocomposite, the storage modulus increased substantially by 1.1 GPa, representing ~33% improvement.

The effect of FSWCNT loading on the glass transition temperature, defined as the peak maximum of tan δ is shown as unfilled symbols in Fig. 6. The glass transition temperature of FSWCNT/epoxy nanocomposites linearly decreased with increasing volume percent of FSWCNT. After adding only 0.071 vol.% (0.1 wt.%) FSWCNT, the glass transition temperature decreased approximately 20 °C. A large decrease in glass transition temperature was not observed with nanocomposites reinforced with organo-clay nanoplatelets [18], silica nanoparticles [19], or vapor grown carbon fibers (as discussed in the next section). The cause of the large reduction of the glass transition temperature with FSWCNT is not known. One possibility is that preferential adsorption of one of the matrix constituents leads to non-stoichiometric balance which would result in depression of the glass transition temperature. The glass transition temperature decreased to near room temperature for the 0.36 vol.% FSWCNT. Indeed, additional increases in storage modulus were not observed beyond 0.21 vol.%. It can be envisioned that even greater amounts of FSWCNT will cause further depression of T_g, leading to a nanocomposite with a T_g below room temperature. When this occurs, it could result in the nanocomposite operating in a temperature plateau where additional improvement in modulus would be minimal above T_g, irrespective of the amount of FSWCNT in the nanocomposite.

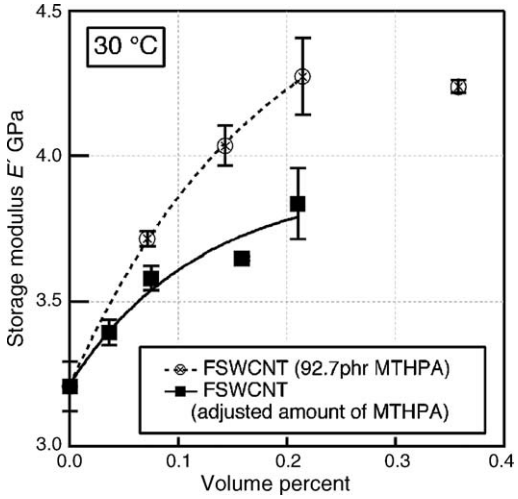

Fig. 5. Storage modulus at 30 °C of anhydride-cured epoxy nanocomposites vs. volume content of FSWCNT.

To investigate the effects of stoichiometric balance on matrix and nanocomposite properties, the amount of MTHPA was adjusted between 60 and 92.7 phr. In this set of specimens, the weight content of FSWCNT became larger when the amount

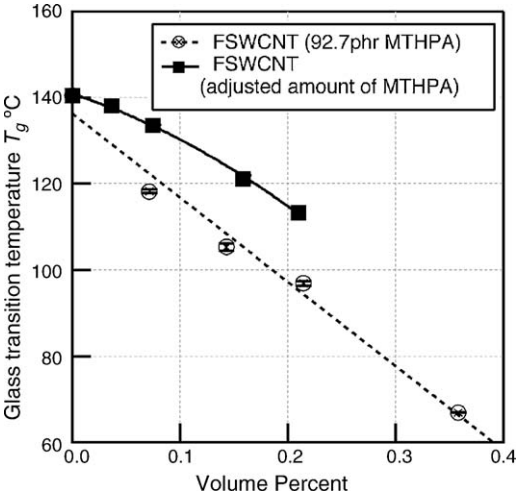

Fig. 6. Glass transition temperature of anhydride-cured epoxy nanocomposites vs. volume content of FSWCNT.

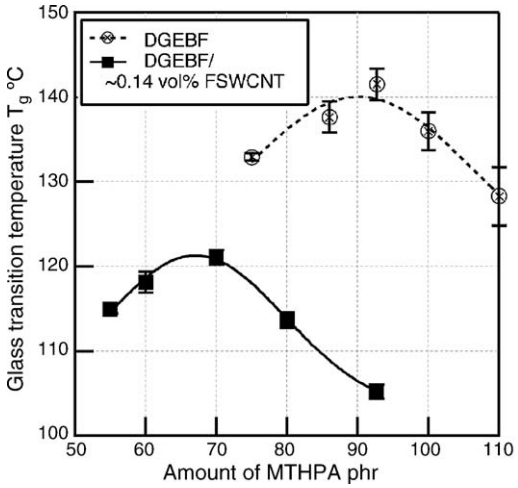

Fig. 7. Dependence of glass transition temperature on concentration of anhydride curing agent.

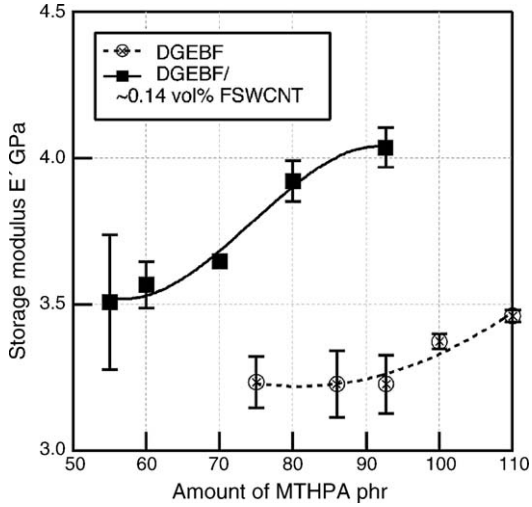

Fig. 8. Dependence of storage modulus on concentration of anhydride curing agent.

of MTHPA was reduced. Fig. 7 shows the relationship between the amount of anhydride curing agent and the glass transition temperature. It is known that the glass transition temperature is maximized at the stoichiometric ratio of curing agent to epoxide functionality [20]. The solid curve in this figure shows the average experimental values for FSWCNT/epoxy nanocomposites and their least-square fit, having a maximum at approximately 67 phr MTHPA. The dashed curve in Fig. 7 shows the average experimental values for neat epoxy, which has a peak glass transition temperature at 92.7 phr MTHPA. This suggests that the addition of 0.14 vol.% (0.2 wt.%) FSWCNT causes a depression of glass transition that would occur with a change in MTHPA of nearly 26 phr from the optimal amount. It should also be noted that the glass transition temperature of the 0.14 vol.% FSWCNT nanocomposites was still lower than that of the neat epoxy. Zhao et al. [21] observed a significant change in the infrared absorption spectra and electrical resistance of FSWCNT at 150 °C. The change of infrared spectra was observed at different heated temperature, and they concluded that the pristine FSWCNT reverted to SWCNT after annealing at or above 150 °C. In addition, they have measured the change of electrical resistance. After the heat annealing process, the fluorine atoms were removed. As a result, it was found that the highly electrically conductive SWCNT were regained from insulating FSWCNT. The present FSWCNT/epoxy nanocomposites were cured at 160 °C. One possibility is that fluorine free radicals were created during cure processing at 160 °C resulting in chain scission or stoichiometric imbalance resulting in reduction of the glass transition temperature.

From the results presented in Fig. 7, the reduction in anhydride curing agent to maximize the T_g was 26 phr. Assuming that the reduction of MTHPA to maximize T_g is proportional to FSWCNT weight content, the amount of anhydride curing agent was adjusted to process up to 0.3 wt.% (0.21 vol.%) FSWCNT nanocomposites. The mixing weight ratio was:

$$\text{DGEBF} : \text{MTHPA} : \text{imidazole} : \text{FSWCNT} = 100 : M : 1 : x$$

where, M and x are correlated as:

$$M = -66.1x + 92.7 \quad (1)$$

Fig. 8 shows the dependency of the storage modulus with adjusted amounts of MTHPA for both neat epoxy (shown as unfilled symbols) and ~0.14 vol.% (0.2 wt.%) FSWCNT nanocomposites (shown as filled symbols). For the nanocomposites, the mixing ratio between DGEBF, imidazole, and FSWCNT was fixed in this figure. Consequently, the volume (and weight content) of FSWCNT decreased when larger amount of MTHPA was added to the FSWCNT/DGEBF blend. It was found that excess amount of MTHPA, greater than 93 phr, produced storage modulus increases for both neat epoxy and FSWCNT nanocomposites. That is, the nanocomposites processed with excess MTHPA, which causes a slight decrease of FSWCNT volume fraction, demonstrated significant increases in storage modulus. This is attributed to anti-plasticization effects with excess amount of the anhydride curing agent above the stoichiometric ratio.

The filled symbols with solid curve in Fig. 5 present the storage modulus at 30 °C of nanocomposites versus volume fraction of FSWCNT in which the amount of MTHPA was adjusted to maximize T_g using Eq. (1). The storage modulus at 30 °C increased by 0.63 GPa, ~20%, with the addition of only 0.21 vol.% (0.3 wt.%) of FSWCNT. In comparison with the previous work, 1.5 vol.% (2.5 wt.%) of exfoliated clay nanoplatelets were required to achieve the same improvement of the storage modulus [8]. Comparing the FSWCNT/epoxy nanocomposites with the adjusted amount of MTHPA (solid curve) in Fig. 5 to the FSWCNT/epoxy nanocomposites processed with 92.7 phr MTHPA (dashed curve), it can be seen that the difference in storage modulus was less at reduced amounts of MTHPA. It was discussed in Fig. 8 that the excess amount of MTHPA resulted in higher storage modulus due to anti-plasticization effects. Therefore, larger improvement observed as unfilled symbols in Fig. 5 is attributed to the reinforcing effect of well-dispersed FSWCNT as well as anti-plasticization effects of the epoxy matrix.

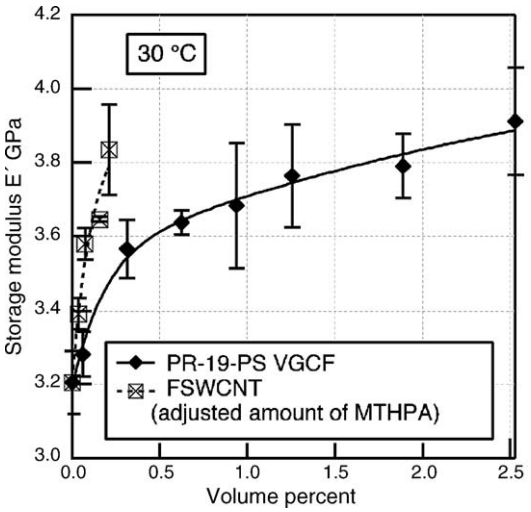

Fig. 9. Storage modulus at 30 °C of anhydride-cured epoxy nanocomposites vs. volume content of VGCF.

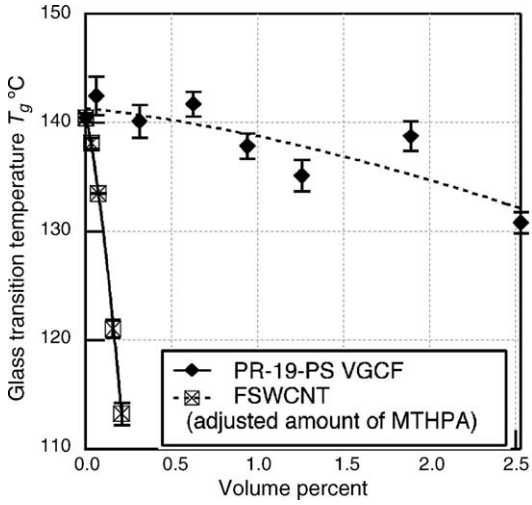

Fig. 10. Glass transition temperature of anhydride-cured epoxy nanocomposites vs. volume content of VGCF.

In Fig. 6, the filled symbols with solid curve show the glass transition temperature of FSWCNT/epoxy nanocomposites after reducing the amount of MTHPA. The decrease of the glass transition temperature was minimized by adjusting the amount of MTHPA. However, the glass transition temperature continued to decrease as the amount FSWCNT in the composites was increased.

3.3. VGCF/epoxy nanocomposites

The relationship between storage modulus at 30 °C and volume content of PR-19-PS VGCF is graphically presented as filled symbols in Fig. 9. The result of FSWCNT/epoxy nanocomposites processed with adjusted amount of MTHPA is also presented as unfilled symbols for reference. The storage modulus of VGCF nanocomposites exhibited a non-linear increase with increasing VGCF content into up to 2.5 vol.% (4.0 wt.%). The storage modulus of the epoxy at room temperature increased 450 MPa, 14%, with the addition of only 0.63 vol.% (1.0 wt.%) of VGCF. As expected, the lower modulus VGCP resulted in a lower composite storage modulus compared with corresponding loading levels of SWCNT. However, the improvement with small amounts of VGCF was greater than that with organo-clay nanoplatelets [12].

Filled symbols in Fig. 10 show the glass transition temperature of VGCF/epoxy nanocomposites at increasing VGCF content. The result of FSWCNT/epoxy nanocomposites processed with adjusted amount of MTHPA is also presented as unfilled symbols for reference. In contrast to the FSWCNT/epoxy nanocomposite where T_g was observed to decrease with increasing weight percent, the glass transition temperature of VGCF nanocomposites slightly decreased with respect to increasing amounts of VGCF. The reason of the T_g decrease was the existence of hydroxyl group on the VGCF surface. An investigation by X-ray photoelectron spectroscopy (XPS) showed that the 4.71 at.% hydroxyl group existed on the VGCF surface. The hydroxyl group could easily reacted with MTHPA, causing a lower cross-link density, and consequently detected as lower T_g.

4. Conclusions

In this study the thermo-physical properties of epoxy nanocomposites reinforced by FSWCNT and VGCF were investigated. The sonication method produced well-dispersed FSWCNT and VGCF in the anhydride-cured epoxy matrix. The glass transition temperature and decomposition temperature of FSWCNT/epoxy nanocomposites decreased with increasing amount of FSWCNT. Adjusting the amount of MTHPA resulted in an improvement in storage modulus and glass transition of FSWCNT/epoxy nanocomposites. The matrix with the adjusted MTHPA levels exhibited ~20% improvement of storage modulus of FSWCNT/epoxy nanocomposites, when incorporating only a 0.21 vol.% of FSWCNT. For VGCF/epoxy nanocomposites, smaller decreases of glass transition temperature was observed with increasing weight fraction. This T_g decrease was caused by the chemical reaction between the hydroxyl group on the VGCF surface and MTHPA, resulting lower cross-link density.

Acknowledgements

A portion of this research was supported under sponsorship of the University of Utah, No. 2103050 as part of a DOE contract entitled, ‘A Multiscale Modeling and Experimental Study of the Mechanics of Polymer Nanocomposite Materials’, John Nairn, P.I. The authors would like to acknowledge Huntsman Advanced Materials Americas Inc. for sample supply. We would also acknowledge the helpful discussion with Dr. Per Askeland at Composite Materials and Structures Center in Michigan State University for X-ray photoelectron spectroscopy.

References

[1] S. Iijima, Nature 354 (1991) 56.
[2] R.S. Ruoff, D.C. Lorents, Carbon 33 (7) (1995) 925–930.

[3] M.M.J. Tracy, T.W. Ebbesen, J.M. Gibson, Nature 381 (1996) 678.
[4] C.F. Cornwell, L.T. Wille, Solid State Commun. 101 (1997) 555.
[5] O. Lourie, D.M. Cox, H.D. Wagner, Phys. Rev. Lett. 81 (1998) 1638–1641.
[6] J.P. Salvetat, G.A.B. Briggs, J.M. Bonard, R.R. Basca, A.J. Kulik, T. Stoeckli, N.A. Burnham, L. Forro, Phys. Rev. Lett. 82 (1999) 944–947.
[7] M.F. Yu, B.S. Files, S. Arepalli, R.S. Ruoff, Phys. Rev. Lett. 84 (24) (2000) 5552–5555.
[8] H. Miyagawa, M.J. Rich, L.T. Drzal, Polym. Compos. 26 (1) (2005) 42–51.
[9] Personal information.
[10] K.N. Kudin, G.E. Scuseria, B.I. Yakobson, Phys. Rev. B 64 (2001) 235406.
[11] Materials properties obtained from Carbon Nanotechnologies Inc. web site: http://www.cnanotech.com/pages/buckytube_properties_uses/buckytube_properties.
[12] J. Zhu, J.D. Kim, H.Q. Peng, J.L. Margrave, V.N. Khabashesku, E.V. Barrera, Nano Lett. 3 (2003) 1107.
[13] D. Penumadu, A. Dutta, G.M. Pharr, B. Files, J. Mater. Res. 18 (2003) 1849.
[14] G.P. Tandon, G.J. Weng, Composite Sci. Technol. 27 (1986) 111.
[15] J.C. Halpin, S.W. Tsai, Air Force Technical Report AFML-TR 67-423, Wright Aeronautical Labs., Dayton, OH, 1967.
[16] C.Y. Hui, D. Shia, Polym. Eng. Sci. 38 (1998) 774.
[17] Material properties obtained from Applied Sciences Inc. web site: http://www.apsci.com/ppi-pyro3.html.
[18] O.L. Blakslee, D.G. Proctor, E.J. Seldin, G.B. Spence, T. Weng, J. Appl. Phys. 41 (1970) 3373–3382.
[19] H. Miyagawa, M.J. Rich, L.T. Drzal, in: Proceedings of the 31st Annual Conference of North American Thermal Analysis Society, 2003, CD-ROM #109.
[20] V.B. Gupta, L.T. Drzal, C.Y.-C. Lee, M.J. Rich, Polym. Eng. Sci. 25 (1985) 812–823.
[21] W. Zhao, C. Song, B. Zheng, J. Liu, T. Viswanathan, J. Phys. Chem. B 106 (2002) 293–296.